PAPER · OPEN ACCESS

Physics-inspired spatiotemporal-graph AI ensemble for the detection of higher order wave mode signals of spinning binary black hole mergers

To cite this article: Minyang Tian et al 2024 Mach. Learn.: Sci. Technol. 5 025056

You may also like

MACHINE LEARNING
Science and Technology

Physics-inspired spatiotemporal-graph AI ensemble for the detection of higher order wave mode signals of spinning binary black hole mergers

Minyang Tian[1,2,3,*] , **E A Huerta**[1,3,4] , **Huihuo Zheng**[5] and **Prayush Kumar**[6]

1 Data Science and Learning Division, Argonne National Laboratory, Lemont, IL 60439, United States of America
2 Department of Physics, University of Illinois at Urbana-Champaign, Urbana, IL 61801, United States of America
3 NCSA, University of Illinois at Urbana-Champaign, Urbana, IL 61801, United States of America
4 Department of Computer Science, The University of Chicago, Chicago, IL 60637, United States of America
5 Leadership Computing Facility, Argonne National Laboratory, Lemont, IL 60439, United States of America
6 International Centre for Theoretical Sciences, Tata Institute of Fundamental Research, Bangalore 560089, India
* Author to whom any correspondence should be addressed.

E-mail: mtian8@illinois.edu

Abstract

We present a new class of AI models for the detection of quasi-circular, spinning, non-precessing binary black hole mergers whose waveforms include the higher order gravitational wave modes $(\ell, |m|) = \{(2,2), (2,1), (3,3), (3,2), (4,4)\}$, and mode mixing effects in the $\ell = 3, |m| = 2$ harmonics. These AI models combine hybrid dilated convolution neural networks to accurately model both short- and long-range temporal sequential information of gravitational waves; and graph neural networks to capture spatial correlations among gravitational wave observatories to consistently describe and identify the presence of a signal in a three detector network encompassing the Advanced LIGO and Virgo detectors. We first trained these spatiotemporal-graph AI models using synthetic noise, using 1.2 million modeled waveforms to densely sample this signal manifold within 1.7 h using 256 NVIDIA A100 GPUs in the Polaris supercomputer at the Argonne Leadership Computing Facility. This distributed training approach exhibited optimal classification performance, and strong scaling up to 512 NVIDIA A100 GPUs. With these AI ensembles we processed data from a three detector network, and found that an ensemble of 4 AI models achieved state-of-the-art performance for signal detection, and reports two misclassifications for every decade of searched data. We distributed AI inference over 128 GPUs in the Polaris supercomputer and 128 nodes in the Theta supercomputer, and completed the processing of a decade of gravitational wave data from a three detector network within 3.5 h. Finally, we fine-tuned these AI ensembles to process the entire month of February 2020, which is part of the O3b LIGO/Virgo observation run, and found 6 gravitational waves, concurrently identified in Advanced LIGO and Advanced Virgo data, and zero false positives. This analysis was completed in one hour using one NVIDIA A100 GPU.

1. Introduction

The development of AI methodologies for gravitational wave astrophysics is a booming enterprise. Since 2017 [1–4], there has been a rapid development of AI methods and approaches to create, test and deploy production scale tools for gravitational wave detection. These novel AI methodologies are being explored in earnest to provide alternatives to well established, though compute intensive and poorly scaling, signal processing tools, such as template matching algorithms, which utilize large sets of modeled waveforms to search for signals in gravitational wave data [5, 6]. The first class of AI models for gravitational wave detection were designed to describe 2D gravitational wave signal manifolds, comprising the masses,

(m_1, m_2), of non-spinning, quasi-circular binary black hole mergers, and which were capable of detecting true gravitational wave signals with a false positive rate of one misclassification for every 100 s of searched data [7–9]. The development of these AI models required training datasets with a few tens of thousands of modeled signals, and a couple of inexpensive GPUs to complete the training within a few hours. These findings sparked the interest of the gravitational wave community, leading to the organic creation of a vibrant, international community of researchers who are harnessing advances in AI and computing to address timely and pressing challenges in gravitational wave astrophysics [10–27]. These seminal ideas have been applied for signal detection [28–30] and forecasting [31–33] of binary neutron stars, and for the detection and forecasting of neutron star-black hole systems [31, 34]. Comprehensive reviews of this active area of research may be found in [35–37], while [38] provides a wider view on other problems tackled in the literature with machine-learning methods such as detector noise characterisation and glitch classification, core-collapse supernovae detection, parameter estimation, etc.

Promoting these disruptive ideas into production scale frameworks for gravitational wave discovery requires innovation at the interface of AI and supercomputing [39]. This is because AI models that describe compact binary systems that may be detectable by ground-based interferometric detectors span a high dimensional signal manifold. Assuming astrophysical compact binary sources that spiral into each other following a series of quasi-circular orbits, and whose individual components are spinning and non-precessing, may be described in terms of four parameters (m_1, m_2, s_1^z, s_2^z). This 4D signal manifold needs to be smartly and densely sampled to train AI models so as to capture the physics of these gravitational wave sources. This then translates into training datasets that have tens of millions of modeled waveforms, i.e. Terabyte size datasets. Therefore, in order to reduce time-to-solution, it is critical to use distributed training algorithms that optimally utilize between hundreds to thousands of GPUs in supercomputing platforms. Furthermore, these methodologies enable the design of AI surrogates that incorporate physics and math principles in their architecture, training and optimization. In parallel to these development, it is essential to create new methods to improve the sensitivity and performance of state-of-the-art AI models.

Recent accomplishments at the interface of physics inspired AI and supercomputing include the design of physics inspired AI architectures, training and optimization schemes that leverage thousands of GPUs [40, 41]. These AI surrogates have been used to process from seconds- to years-long datasets of gravitational wave data to demonstrate that AI can be used to search for and find gravitational wave signals with an average false positive rate of one misclassification for every month of searched data [42, 43]. It has also been demonstrated that when these AI surrogates are optimized for accelerated inference with NVIDIA TensorRT, and the inference is distributed over the entire ThetaGPU supercomputer at the Argonne Leadership Computing Facility, consisting of 160 NVIDIA A100 Tensor Core GPUs, gravitational wave data can be processed over 52, 000X faster than real-time assuming a two detector network comprising the twin Advanced LIGO detectors [44].

Since AI advances in gravitational wave astrophysics exhibit great promise [18, 19, 21, 33, 34, 45–47], in this article we contribute to this line of research by designing AI architectures, training and optimization methods that incorporate physics and geometrical principles involved in the detection of gravitational waves. In practice, we have designed neural networks that capture both short- and long-range temporal dependencies of gravitational wave signals with hybrid dilated convolution networks. We also incorporate geometrical and spatial considerations of signal detection in terms of the location of gravitational wave detectors through graph neural networks. We show that this approach improves the sensitivity of AI ensembles for signal detection, while also reducing the number of false positives to 7 misclassification for every decade of searched data when using an ensemble of two AI models, and to 2 misclassification for every decade of searched data when using an ensemble of 4 AI models. This is the first time AI methods achieve this level of accuracy over decade-long datasets.

We showcase this approach in the context of a network of three ground-based gravitational wave detectors encompassing the twin Advanced LIGO and Advanced Virgo detectors. We present results for an astrophysical population of quasi-circular, spinning, non-precessing binary black hole mergers. We show how to reduce time-to-solution by using distributed training on the Polaris supercomputer at the Argonne Leadership Supercomputing Facility, in which we used 256 NVIDIA A100 GPUs to train AI models within 1.7 h, while also ensuring optimal classification performance. We also demonstrate that our approach presents strong scaling up to 512 NVIDIA A100 GPUs. We also used 128 NVIDIA A100 GPUs in Polaris and 128 nodes in the Theta supercomputer to process a decade's worth of simulated advanced gravitational wave data from a three detector networks within 3.5 h, i.e. 25 000X faster than real-time.

2. Results

We present a novel approach that brings together physical and geometrical considerations in the design and training of AI models for gravitational wave detection. We use a hybrid dilated convolution network (HDCN) to capture long-range temporal dependencies that are crucial for signal prediction, and combine it with a graph neural network (GNN) to merge prediction embeddings from a three detection network—Advanced LIGO Livingston (L) and Hanford (H); and Advanced Virgo (V)—considering their spatial relationship.

We used the IMRPhenomXPHM waveform approximant [48] to model signals that include the higher-order wave modes $(\ell, |m|) = \{(2, 2), (2, 1), (3, 3), (3, 2), (4, 4)\}$, and mode mixing effects in the $\ell = 3$, $|m| = 2$ harmonics for quasi-circular, spinning, non-precessing binary black holes. Given the large amount of modeled waveforms needed to optimally sample this signal manifold, we introduce novel approaches to train these AI models at scale in modern computing environments. We showcase how to use these AI models to search for modeled waveforms in synthetic, recolored noise; as well as in real gravitational wave data from the third Observing Run (O3) taken from the Gravitational Wave Open Science Center [49]. To the best of our knowledge, these are the first type of AI models designed to search for higher order gravitational wave modes in real gravitational wave data.

In the Methods section we describe in detail the datasets and modeled waveforms used for these studies, and approaches we have developed to train AI models at scale, and to enable hyper-efficient AI inference of large scale gravitational wave datasets in leadership class supercomputers.

We present results that quantify the ability of our AI models to search for and find gravitational waves in a decade-long gravitational wave dataset in which we consider a three detector network comprising the twin Advanced LIGO detectors and the Advanced Virgo detector, assuming an astrophysical population of quasi-circular, spinning, non-precessing binary black hole mergers.
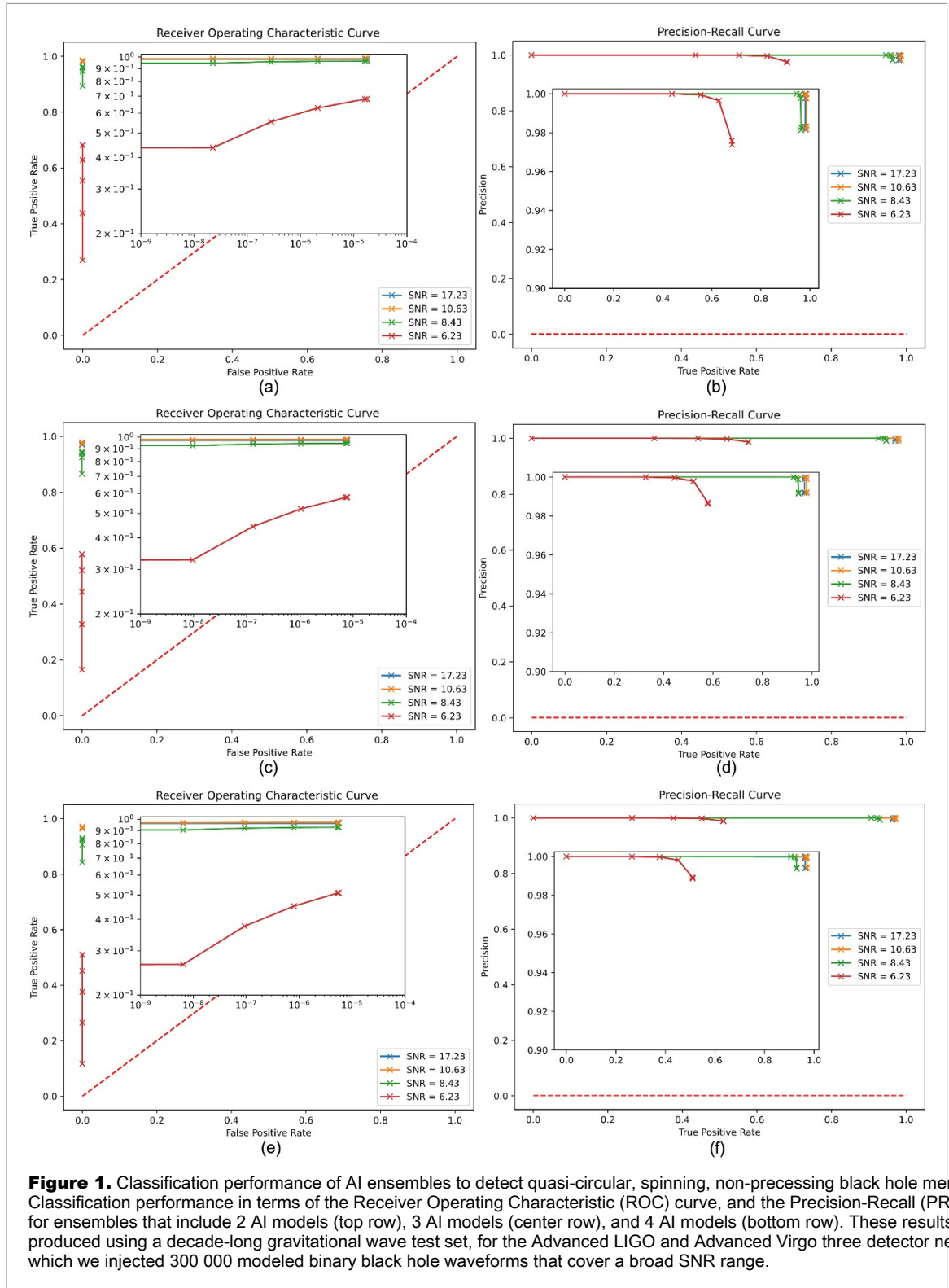
2.1. Quasi-circular, spinning, non-precessing binary black hole mergers

We consider a binary black hole population described by 4 parameters, namely (m_1, m_2, s_1^z, s_2^z). The individual masses span the range $m_{1,2} \in [3 M_\odot, 50 M_\odot]$, while their individual spins cover the range $s_{\{1,2\}}^z \in [-0.9, 0.9]$. To instill the physics of these astrophysical sources into our AI surrogates, we have produced datasets of modeled waveforms using the IMRPhenomXPHM model [48], which we used to incorporate higher order wave modes in the modeling of binary black hole mergers. We also used this model since it facilitates the production of modeled waveforms at scale in modern computing environments. Here, we used three independent, non-overlapping datasets: the training dataset has 1.2 million waveforms, whereas the validation and test sets have 300 000 modeled waveforms.

These waveforms are then curated to simulate a variety of astrophysically motivated scenarios. We do this by using tools provided by the open-source PyCBC library [50] to uniformly sample the masses and individual spins of binary components, as well as the various angles that describe the sky location of these sources, except for the inclination angle for which we use a sin (inclination) distribution. For signal-to-noise ratios (SNRs) we use a uniform volume prior. This approach ensures that AI models are capable of correctly identifying gravitational waves that may be produced in a wide variety of astrophysical scenarios. Once our AI models are fully trained, we test them with new datasets that have not seen by these AI models during training. These new datasets contain either pure noise, or noise plus injected signals that simulate detection scenarios. Figure 1 presents two types of metrics we used to quantify the performance of our AI models for signal detection, i.e. the Receiver Operating Characteristic (ROC) curve and the Precision-Recall (PR) curve. Therein we present results for three cases, in which we construct ensembles that include, 2 AI models (top row), 3 AI models (center row), and 4 AI models (bottom row), respectively.

To create the ROC curve, we computed the true positive rate against the false positive rate as estimated from the output of our AI ensembles when we use them to process a decade-long dataset that describes a three detector network that comprises the Advanced LIGO and Advanced Virgo detectors. As mentioned before, the test set includes 300 000 modeled waveforms to quantify the ability of AI ensembles to correctly identify modeled waveforms, and discard other noise anomalies. To produce the PR curve, we consider that PR = TP/ (TP + FP), where TP and FP stand for True Positives and False Positives, respectively. Key results we extract from these studies include the following:

- Figure 1 shows that AI's precision to detect gravitational waves improves as we increase the number of AI models in the ensemble (right column). At the same time, there is a marginal reduction in the true positive rate, in particular for low SNR signals (both left and right column).
- We provide key figures of merit in table 1 Therein we show that a 2 AI model ensemble reports 7 false positives per decade, a 3 AI model ensemble reports 3 false positives per decade, while a 4 AI model ensemble produces 2 misclassifications per decade of searched data. We also present the Area Under the Curve (AUC)

Figure 1. Classification performance of AI ensembles to detect quasi-circular, spinning, non-precessing black hole mergers. Classification performance in terms of the Receiver Operating Characteristic (ROC) curve, and the Precision-Recall (PR) curve for ensembles that include 2 AI models (top row), 3 AI models (center row), and 4 AI models (bottom row). These results were produced using a decade-long gravitational wave test set, for the Advanced LIGO and Advanced Virgo three detector network, in which we injected 300 000 modeled binary black hole waveforms that cover a broad SNR range.

for the ROC and PR curves for gravitational wave signals in our 300 000 test set with cumulative three detector network SNR_1 = 8.4 and SNR_2 = 10.6. We selected these cumulative three detector network SNR values since they provide a fair representation of the bulk of events reported in the Gravitational Wave Open Science Center [51]. These results show that as we consider larger AI ensembles there is marginal decrease in the ROC AUC and PR AUC for low SNR signals, while signals with SNR_2 8.4 have a negligible change.

This work significantly outperforms recent results in the literature [43, 44], in which AI models were used to process a 5 year-long dataset. Here we significantly improve the classification performance of those AI models, both in terms of improving the true positive rate for signals across SNRs, and with a very significant

Table 1. Classification performance of AI ensembles that include 2, 3 or 4 AI models (left column). Here we consider a population of quasi-circular, spinning, non-precessing binary black hole mergers. FP presents the number of false positives reported by the AI ensembles upon processing a decade-long gravitational wave test set that describes a three detector network comprising the Advanced LIGO and Advanced Virgo detectors, and in which we injected 300 000 modeled waveforms that cover a broad range of signal-to-noise ratios (SNRs). We also present additional figures of merit, namely, the Area Under the Curve (AUC) for the Receiver Operating Characteristic (ROC) curve, and the Precision-Recall (PR) curve for two cumulative three detector network SNR values that represent the bulk of events detected thus far by Advanced LIGO and Advanced Virgo, i.e. $SNR_1 = 8.3$ and $SNR_2 = 10.6$—see also figure 1.

# of models	FP	ROC AUC		PR AUC	
		SNR_1	SNR_2	SNR_1	SNR_2
2	7	0.9818	0.9929	0.9636	0.9857
3	3	0.9730	0.9894	0.9460	0.9789
4	2	0.9649	0.9855	0.9297	0.9710

improvement for low and moderate SNR signals (compare these findings to those in figure 4 in [43]). We also reduce the number of misclassifications from 1 per month to 2 per decade. This is the first time AI reaches this level of accuracy to correctly tell apart gravitational waves from other noise anomalies.

In brief, AI ensembles trained with modeled waveforms that describe quasi-circular, spinning, non-precessing binary black hole mergers provide optimal results. This is because these AI models are exposed to signals with more complex morphology and time-evolution, and thus are better equipped at telling apart true signals from other noise anomalies. Again, if compare these results to those presented in [43, 44], we notice that the AI models and computational methods we introduce in this paper significantly improve the capabilities of AI for signal detection by enhancing its precision and accuracy, and by significantly reducing the number of false positives over long datasets.

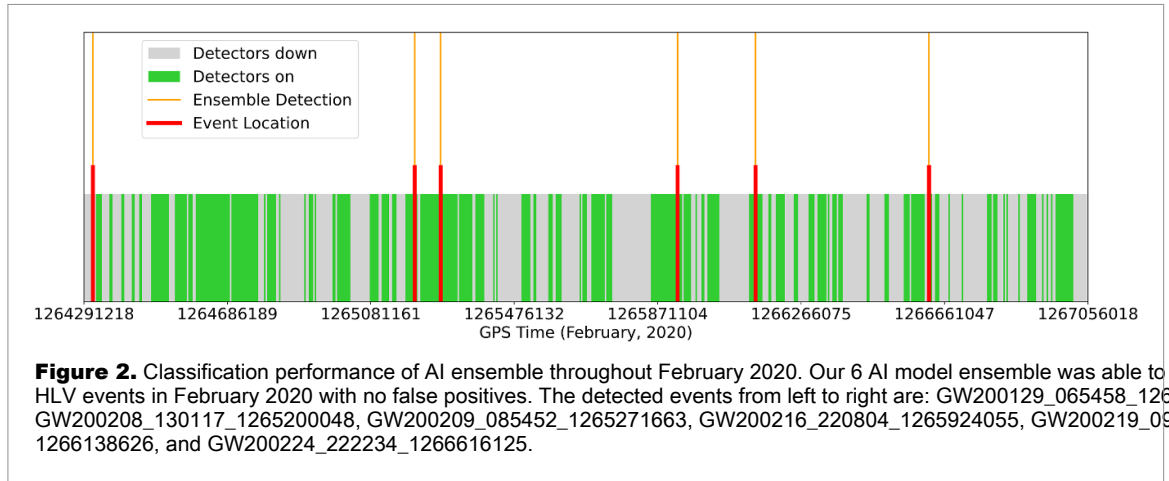## 2.2. Results with synthetic noise: trends and patterns

In the results above, we notice that there is a trade-off in true positive rate and false positive rate that is driven by the size of the ensembles. As we increase the number of AI models, the precision increases, i.e. we find less false positives. At the same time, the true positive rate also marginally decreases. Another factor at play here is that we are combining several AI models that share the same architecture, and whose initial weights have been randomly initialized for training and optimization. These three factors affect the ROC AUC and PR AUC. Note, though, that these differences are ⩽3%, which is well within the range of fluctuations in performance due to training and optimization.

2.3. AI ensembles on O3b data

In the results presented above, we considered a detector network whose individual components have comparable sensitivity. We now explore the application of our AI ensembles for O3b gravitational wave data, in which the H, L and V detectors reported a binary neutron star inspiral range of 135 Mpc, 115 Mpc, and 50 Mpc, respectively [52]. These disparate sensitivities mean that our AI models will now have to deal with two input channels that provide comparable outputs, HL, while another channel, V, will provide noisier outputs. Since our AI architecture aggregates the output predictions from each H, L and V detector, this means that our AI models may get confused when H&L predictions agree on the existence of a potential event, while V may flag it inconsistently as a positive or negative sample. Notwithstanding these significant changes in the original scope and design of our AI models, we have fine-tuned our AI models to search for HLV events in O3b data.

In practice, we selected O3b data covering the GPS times 1264291218 through to 1267056018. For training purposes, we extracted three separate L, H, and V data segments, which are 4096 s long, and have the following GPS start times: 1264685056, 1265528832 and 1266200576. We estimated training PSDs for L, H, and V using these three 4096 s long segments. To produce AI ensembles with real data, we considered the training dataset of 1.2 million higher order wave modes that describe quasi-circular, spinning, non-precessing binary black hole mergers.

We then fine-tuned a suite of 20 AI models with these real datasets. Each of these models was fine-tuned within 320 min using 48 NVIDIA A100 GPUs in the Polaris supercomputer. We selected the top 6 AI classifiers and used them to process data from February 2020. Our findings indicate that this AI ensemble can identify the following 6 gravitational wave events: GW200129_065458_1264314069, GW200208_130117_1265200048, GW200209_085452_1265271663, GW200216_220804_1265924055, GW200219_094415_1266138626, and GW200224_222234_1266616125. Our AI ensemble also reported no false positives, as shown in figure 2.

Figure 2. Classification performance of AI ensemble throughout February 2020. Our 6 AI model ensemble was able to identify 6 HLV events in February 2020 with no false positives. The detected events from left to right are: GW200129_065458_1264314069, GW200208_130117_1265200048, GW200209_085452_1265271663, GW200216_220804_1265924055, GW200219_094415_1266138626, and GW200224_222234_1266616125.

2.4. Quantitative comparison to other signal detection pipelines with real data

We can readily compare the output of our AI ensemble with other established pipelines for gravitational wave detection for the O3b data we analyzed above. These results are summarized in table 2. It is worth pointing out that while the template-matching and template-agnostic pipelines listed in table 2 benefit from additional information such as data calibration, data quality information, and data cleaning, our AI ensembles are trained, validated and tested using available data at the Gravitational Wave Open Science Center [49]. Thus, we have carried out an additional comparison between PyCBC and our AI ensemble using open source data as is.

To carry out this analysis, we analyzed 4096 s of HLV data around each of the ten events reported in [52] for O3b data covering the GPS times 1264291218 through to 1267056018. Using PyCBC version 32498060a5ef01fad606fe0a3e28b1a632adff30 (6 November 2023), we computed the matched-filtering integral from 20 Hz with the data and templates being sampled at 2048 Hz. We used IMRPhenomD waveform templates [53] with a bank that covers the black hole mass range $m_{1,2} \in [3M_\odot, 50M_\odot]$, and aligned individual spins $\chi^z_{1,2} \in [-0.9, 0.9]$ with a minimal match of 97%. The search estimates the noise Power Spectral Density (PSD) over 512 s chunks of data, and takes the median over all chunks. Other technical details, including the ranking statistic used and methodology to compute the significance of triggers are as used in LVK analyses [52]. Note that our AI ensemble is designed to consider aligned individual spins *and higher order modes*, which are not considered in PyCBC since it would considerably increase its computational cost.

The PyCBC runs for each of the 4096 s long segments include filtering, coincidence finding, ranking of events, and a small number of injections to determine the horizon range of the search. Each individual analysis was completed in 4.5 h using 4 CPUs with 8GB RAM. AI inference on each of these segments was completed in 20.95 s with one NVIDIA A100 GPU. We summarize the findings of this analysis in table 3. Therein we notice that our AI ensemble can identify 6 HLV gravitational wave events with no misclassifications. PyCBC can identify 3 gravitational wave events, and each has a sizeable list of false positives, which are directly provided by PyCBC, and correspond to coincident triggers present in all three detectors, HLV, that have a minimum individual detector SNR of 5. We took a closer look at the 4 events that our AI ensemble did not find, and discovered that:

- GW200202_154313_1264691364. According to [52], this event had individual detector SNR of 4.6, 10, and 2.4 for H, L, and V, respectively, for the GstLAL pipeline [6]. Since our AI model aggregates the predictions from the three detector outputs, this event went unnoticed for both the H and V nodes, and thus marked as noise.
- GW200208_222617_1265233948. As before, according to [52], this event had individual detector SNR of 5.6, 5.7, and 2.1 for H, L, and V, respectively, for the GstLAL pipeline [6]. This event went unnoticed for V and thus marked as noise.
- GW200210_092254_1265359745. This is a neutron star-black hole system, outside of the parameter space that we considered in this study.
- GW200220_061928_1266212739. The masses of this event are out of the range we considered to train our AI models.

In brief, this analysis indicates that our AI ensembles may greatly benefit from using additional information to further increase their detection capabilities, i.e. data quality information, data cleaning, and other

Table 2. HLV events detected by six different detection pipelines using data from the O3b run throughout February 2020. Note that single detection triggers are not included here.

HLV Events	AI	cWB	GstLAL	MBTA	PyCBC-broad	PyCBC-BBH
GW200129_065458_1264314069		3			3	3
GW200208_130117_1265200043		3	3		3	3
GW200209_085452_1265271663		3	3		3	3
GW200216_220804_1265924055		3	3		3	3
GW200219_094415_1266138626	3	3	3		3	3
GW200224_222234_1266616125	3	3	3		3	3

Table 3. Signal detection comparison between our AI ensemble and PyCBC analyses for 10 events reported in [52] for O3b data covering the GPS times 1264291218 through to 1267056018. The data used for this analysis is open source data available at the Gravitational Wave Open Science Center [49].

HLV Events	AI	# False Positives	PyCBC	# False Positives
GW200129_065458_1264314069		0	3	307
GW200202_154313_1264691364		0		239
GW200208_130117_1265200043		0	3	284
GW200208_222617_1265233948		0		323
GW200209_085452_1265271663		0		291
GW200210_092254_1265359745		0		290
GW200216_220804_1265924055		0		284
GW200219_094415_1266138626		0		219
GW200220_061928_1266212739		0		231
GW200224_222234_1266616125		0	3	273

methodologies used in established gravitational wave detection pipelines. We also learn that AI methods already provide the means to search for gravitational wave signals with very complex morphology at minimal computational cost.

3. Methods

Here we describe in detail the datasets, AI architectures, training and optimization schemes used to create our AI models.

3.1. Datasets

We used the IMRPhenomXPHM waveform model [48] to create datasets of modeled waveforms, sampled at 4096 Hz, that describe an astrophysical population of binary black holes that spiral into each other following a series of quasi-circular orbits. Their binary components span the masses $m_{1,2} \in [3M_\odot, 50M_\odot]$, and individual spins $s_{1,2} \in [-0.9, 0.9]$. We generated 1.8 million waveforms by uniformly sampling this (m_1, m_2, s_1^z, s_2^z) parameter space. Furthermore, we incorporated information about the sky location and detector location into the modeled waveforms by sampling right ascension and declination, orbital inclination, coalescence phase, and waveform polarization. Right ascension and declination are sampled uniformly on a solid angle of a sphere. The polar angle varies from $\pi/2$ (north pole) to $-\pi/2$ (south pole). The orbital inclination is sampled using a sin(inclination)-distribution. The coalescence phase and waveform polarization are both uniformly sampled covering the range $[0, 2\pi]$. We have densely sampled these parameters to expose our AI surrogates to a broad range of plausible detection scenarios. With this approach our AI surrogates learn the interplay between these parameters, and the slightly different times at which the merger event (waveform amplitude peak) is recorded by our AI surrogates in their three input data channels, representing the Advanced LIGO and Advanced Virgo detectors.

For the construction of AI ensembles using real data, we also consider modeled waveforms that describe higher order wave modes for quasi-circular, spinning, non-precessing binary black hole mergers.

Out of the 1.8 million waveforms in our dataset, we have created three independent, non-overlapping datasets. The training set has 1.2 million waveforms, whereas the validation and test sets have 300 000 modeled waveforms each. In practice, we produced HDF5 files each containing 2000 modeled waveforms that uniformly sampled the parameter space with random variable samples. We then split these files into training, validation and test sets, ensuring that they provide a fair coverage of the parameter space. We follow best machine learning practices and ensure that the recolored noise and signals used to produce the training, validation and test sets are different to each other.

3.2. Power spectral density for Advanced LIGO and Advanced Virgo

To model the sensitivity of Advanced LIGO and Advanced Virgo detectors, we rely on PSD curves. Specifically, we use PSD curves from Advanced LIGO Sensitivity (190 Mpc) based on the fourth observing run (O4, aligo_O4high.txt) for the Hanford and Livingston detectors. For Advanced Virgo detector, we use PSD data from the fifth observing run (O5, avirgo_O5low_NEW.txt), which has a low noise and high range limit target sensitivity [54, 55]. We selected these PSDs to study detection scenarios in which the LIGO and Virgo detectors have similar sensitivities, which may be attained by the end of O5. As we also show below, if one considers O3b PSDs, then the Advanced LIGO and Advanced Virgo detectors have rather disparate sensitivities and the AI models get confused when a noise trigger is found in LIGO data streams (L & H), whereas the same noise trigger in Virgo data is inconsistently labeled by the AI models, especially for moderate SNR signals, given the current noisier nature of Advanced Virgo datasets.

In the context of real gravitational wave data, we estimated training PSDs for the H, L and V detectors using three 4096 s long segments with GPS start times 1264685056, 1265528832 and 1266200576. These segments do not contain any known gravitational wave signals. Following best machine learning practices, the training, validation and test sets are independent, i.e. there is no overlap among them in terms of the simulated signals and real gravitational wave noise used in each of these datasets.

3.3. Data curation

Modeled waveforms were whitened with the aforementioned PSDs. We also produced synthetic noise, and colored it with the PSDs representing each of the detectors. To address the challenge posed by highly imbalanced data in real detection, our dataset uses 70% negative samples (only noise) and 30% positive samples (noise and signals).

For generating negative samples in our model, we randomly select 1 s-long segments of pure noise from the generated synthetic noise. These negative samples are labeled as pure 0 s. On the other hand, for generating positive samples, we consider the whitened signal to the 0.5 s before the merger and the ringdown part. Thereafter, we linearly mixed whitened waveforms and whitened noise so as to describe a broad range of astrophysical scenarios. The label for positive samples will be set to 1 only for the 0.5 s before the merger while the remaining part will be labeled as 0, since we are mostly interested in the merger portion of the signals where the AI models have the sharpest response.

For data curation in the context of gravitational wave data, we follow the same exact procedure with the exception that now we use real H, L and V data to noise-contaminate modeled waveforms, and we whitened both signals and noise using the PSDs that we estimated with real data.

3.4. AI model architecture

Our neural network model has two building blocks: the HDCN block, and the GNN block, which generates the final prediction with an output layer. Our HDCN block is inspired by WaveNet [56], a deep neural network for audio generation tasks, such as human speech or music. It uses dilated causal convolutions to model the temporal dependencies of audio signals, allowing it to generate high-fidelity audio with long-range structure. We believe we can also use it for our high sample rate time-series data, as the dilated convolution layers enable the network to capture larger receptive fields using fewer parameters. Moreover, it block-based structure enables the model to respond to a diverse range of frequency bands.

We present the hybrid dilated convolution structure in figure 3. It consists of pre-processing and post-processing time-distributed convolution layers and dilated convolution layers. With time-distributed convolution layers, HDCN is able to enlarge the expressiveness of the embedding. By stacking dilated convolution layers with different dilation rates and gated activation unit, HDCN will get an exponential increase in the size of the receptive field with respect to the number of layers. It will be crucial when considering long-range temporal dependencies in our signals. Finally, residual structure and skip connections are used to combine both long-range and short-range dependencies. Every detector strain data will be processed by an i.i.d. HDCN block to output the prediction embeddings since we want to preserve each detector's own information for the following GNN block.

On the other hand, there are various GNN structures available [57–61], and we decided to use the Message Passing Neural Network framework with max pooling as the permutation invariant operator. We believe this can help capture the most important features in the embeddings and discard the less significant ones. Additionally, max pooling can help make the model more robust to small perturbations or noise in the input data by focusing on the strongest features, i.e. on the merger event.

Following the HDCN blocks, we obtain three prediction embeddings from the three detector channels. Since all three embeddings should represent the same true signal generated by the binary black hole merger, we need to combine them to produce the final prediction output. While a naive approach is to concatenate the three channels and pass them through a multi-layer perceptron (MLP) [42], this method is not entirely

optimal. If we change the order of the channels, the MLP output will differ even though the channels still represent the same signal. Therefore, we need a more robust approach to combine the embeddings. We use GNN to preserve the permutation invariance between the three detector embeddings and obtain a graph-level embedding as the combined output.

The GNN structure is shown in figure 4(a). For each target node, the GNN block applies an Aggregate step and a Combine step. During the Aggregate step, the GNN processes each neighbor embedding using a convolution layer and then uses max pooling to output the aggregated neighbor message, which is permutation invariant. In the Combine step, the GNN concatenates the aggregated neighbor message with the target node embedding and passes the result to another convolution layer to update the target node embedding. The Aggregate and Combine layer is shared among the 3 nodes. Next, we use max pooling to combine the 3 node embeddings and generate a graph-level embedding. Finally, we apply an MLP with sigmoid activation to the graph-level embedding to generate element-wise predictions.

In the GNN block, we represent each time step as a three-node graph and use the GNN to combine the three embeddings of each time step. Since each time step already encompasses a long receptive field after HDCN, see figure 4(b), this method is sufficient to generate accurate predictions at each time step. We can easily incorporate multiple-step correlation by increasing the kernel size of the convolution layer accordingly. Then, we apply a general GNN to process the node embeddings, as it captures the relationship between the embeddings, i.e. the locations of the detectors. Since the detector locations remain constant over time, we use the same GNN function for all time steps. We can relax this assumption when we consider signals whose detector antenna patterns evolve over time. This approach has the added benefit of preserving the strong correlation between the embeddings, which is due to their highly overlapping receptive fields. Consequently, we can maintain this correlation in our final time-series prediction output. We can consider each time step as a subgraph in a larger graph, as shown in figure 4(c), allowing us to share the aggregation and combination functions across all time steps. In other words, we propose a time-independent GNN to process the time-series embeddings.
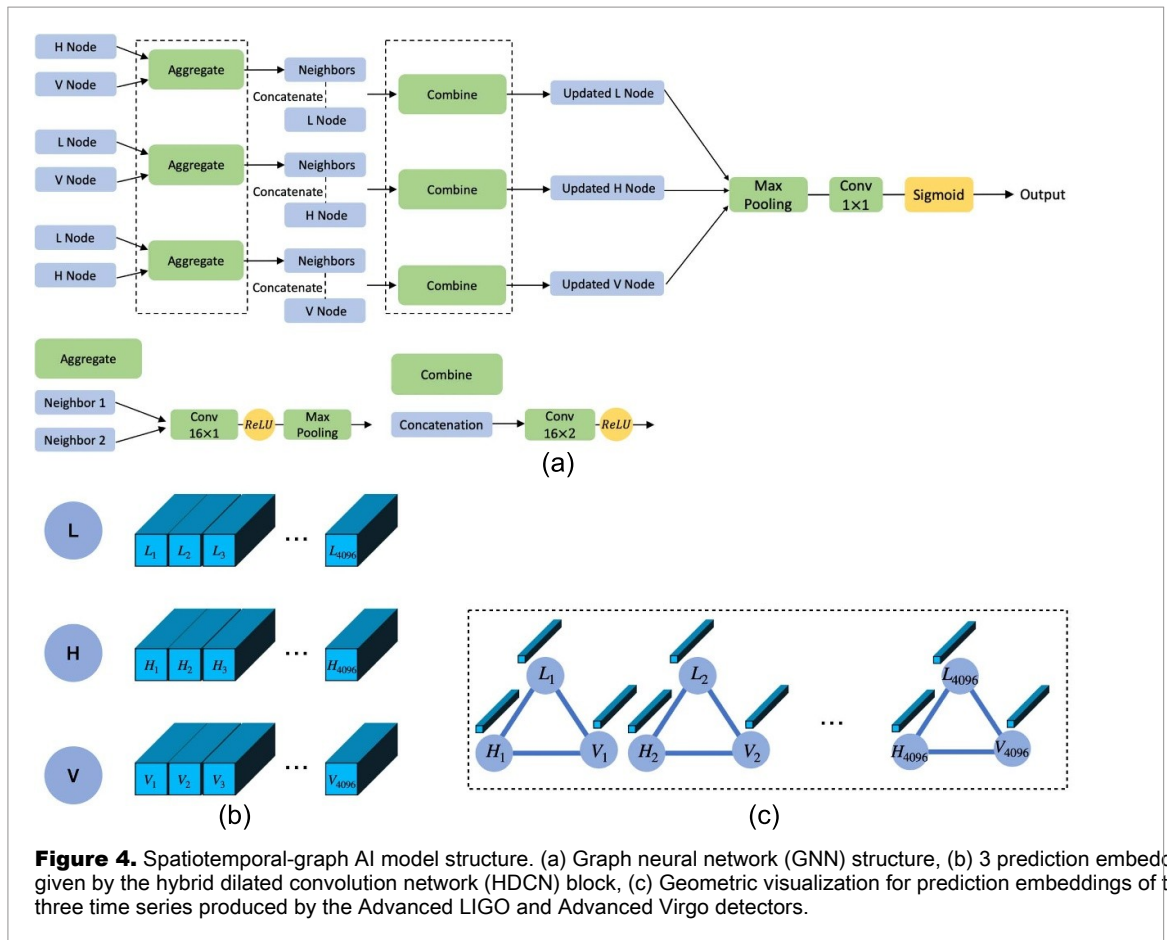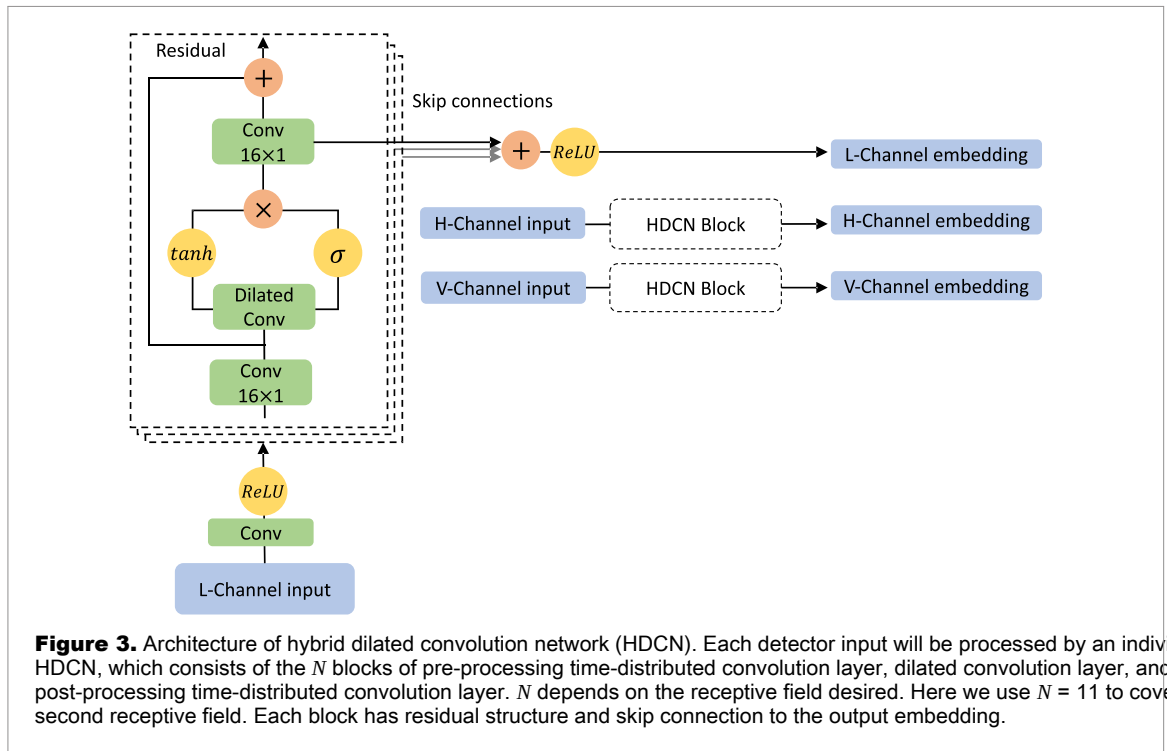
3.5. AI ensembles

Our ensemble method employs a cascading strategy where detection is considered positive, i.e. a real signal or an injected signal, only if there is unanimous agreement among all models. Conversely, if even a single model identifies the detection as negative, i.e. pure noise, the ensemble treats the entire detection as negative. This stringent criterion for positive detection is designed to minimize FPs, ensuring that only the most reliable detections are classified as positive. By requiring consensus, this approach aims to enhance the specificity of our system, effectively reducing the likelihood of false alarms without significantly compromising the sensitivity. This method leverages the strengths of multiple models, filtering out less confident predictions, thereby achieving a balance between sensitivity and specificity that is crucial for maintaining high performance in our application. In practice, when we consider AI models trained, valiated, and tested with synthetic noise, we find that AI ensembles with one, two, three, and four AI models produce 599, 7, 3, and 2 FPs when tested over a decade long dataset.
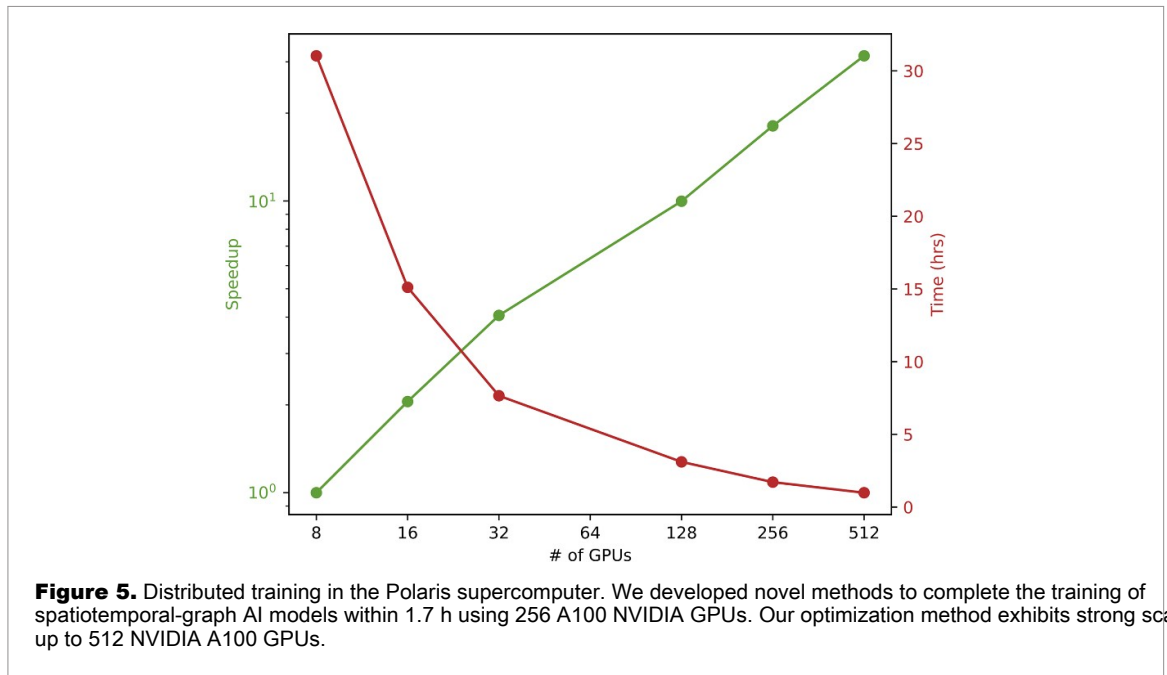
3.6. Detection strategy

For the determination of the threshold used in calculating FPs, we strategically select the threshold that corresponds to the point on the ROC curve nearest to the top left corner, i.e. closest to the point (0,1), which is used to determine the width and height of the find_peaks algorithm, where we choose 0.5 s for the width and a threshold of 0.999 999 for the height of the peak. This decision is grounded in the empirical observations from our validation dataset, where our model demonstrates a strong capability in identifying positive cases even at lower SNR levels, yet accompanied by a considerable number of FPs. Given this performance characteristic and the anticipation of encountering more pronounced data imbalance in real scenarios—predominantly featuring negative or pure-noise samples—we opted for a threshold embodying near-absolute confidence. This stringent threshold criterion aims to substantially minimize false positives, enhancing the precision of our model in real-world applications where the rarity of true positives necessitates a highly cautious approach to declaring positive detections. This method of threshold selection, while potentially increasing the model's specificity, is a deliberate choice to ensure the reliability and applicability of our model's outputs, especially in contexts where the cost of false positives is high and the occurrence of true positives is exceptionally rare.

3.7. Distributed training at scale

We use data parallelism, but not model parallelism, for both training and inference since our model can be fit into a single A100/V100 GPU. In the training stage, data parallelism can help accelerate training time. By distributing the workload across several GPUs, data parallelism significantly reduces the time required for

Figure 3. Architecture of hybrid dilated convolution network (HDCN). Each detector input will be processed by an individual HDCN, which consists of the *N* blocks of pre-processing time-distributed convolution layer, dilated convolution layer, and the post-processing time-distributed convolution layer. *N* depends on the receptive field desired. Here we use *N* = 11 to cover a half second receptive field. Each block has residual structure and skip connection to the output embedding.

Figure 4. Spatiotemporal-graph AI model structure. (a) Graph neural network (GNN) structure, (b) 3 prediction embeddings given by the hybrid dilated convolution network (HDCN) block, (c) Geometric visualization for prediction embeddings of the three time series produced by the Advanced LIGO and Advanced Virgo detectors.

training. This acceleration is crucial for our large datasets, where single-GPU training would be prohibitively slow. Also, the framework for data parallelism is inherently scalable. It can accommodate additional GPUs without major changes to the training algorithm, allowing for linear or near-linear speed-ups with increased hardware resources.

Figure 5. Distributed training in the Polaris supercomputer. We developed novel methods to complete the training of spatiotemporal-graph AI models within 1.7 h using 256 A100 NVIDIA GPUs. Our optimization method exhibits strong scaling up to 512 NVIDIA A100 GPUs.

We conducted scaling tests in the Polaris supercomputer at the Argonne Leadership Computing Facility. In figure 5 we present our scaling results. The AI models presented in this article were trained within 1.7 hrs using 256 A100 GPUs. All these models have optimal classification accuracy. We also conducted scaling studies using up to 512 A100 GPUs, in which case the training phase was completed 59 min. The AI models presented in this paper are the top classifiers, in terms of ROC and PR analyses, from this training campaign. In the context of AI models trained to find events in real data, we fine-tuned a suite of 20 AI models using H, L and V data. This fine-tuning process was completed, for each AI model, within 320 min using 48 NVIDIA A100 GPUs. We then used the same figures of merit described above, such as ROC AUC and PR AUC to identify the top six AI classifiers that we used for AI inference.
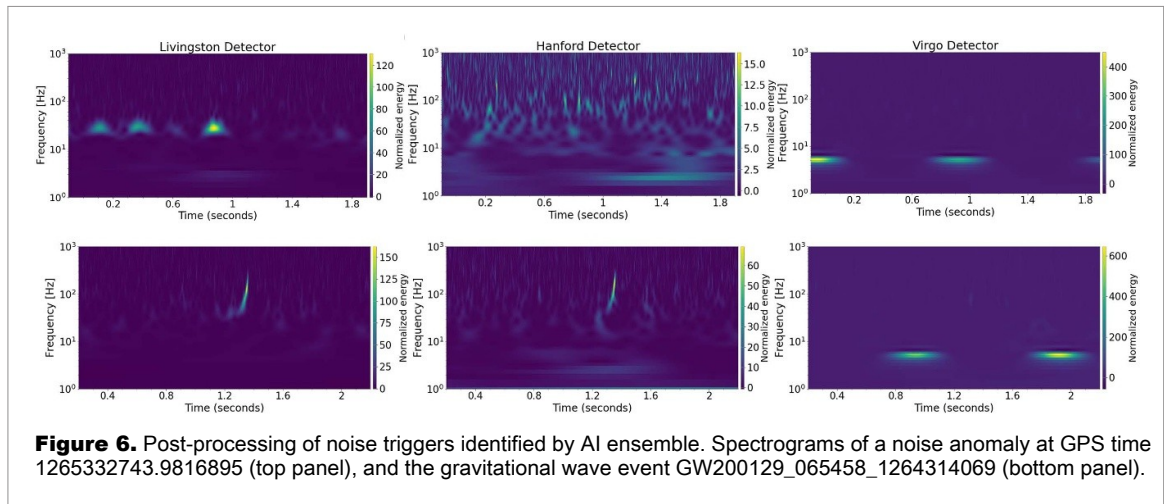
3.8. AI inference at scale

Once we completed the training of multiple AI models with optimal classification performance, we distributed the inference over a decade of simulated gravitational wave data. Leveraging data parallelism during the inference phase allows us to simultaneously distribute data across multiple GPUs, facilitating real-time detection capabilities. This approach not only enhances the throughput of our system by making efficient use of available GPU resources but also significantly reduces latency, ensuring that predictions are generated swiftly and accurately. By parallelizing the data processing workload, we can handle larger volumes of data in real time, maintaining high performance even under heavy load conditions. We first processed these data using our AI ensemble using 128 A100 GPUs in Polaris, and then post-process the AI models' output using 128 CPU nodes in the Theta supercomputer. The first part is completed within 3.19 h, while the second is completed in about 0.3 h. Thus, a decade's worth of gravitational wave data is processed within 3.5 h.

3.9. AI inference on O3b data

We used an additional step to process real data. First we processed the entire month of February 2020 with our ensemble of 6 AI models. This analysis was completed within 1 h using a single NVIDIA V100 GPU. AI inference identified 13 noise triggers, which we then followed up using Data Quality tools provided by the Gravitational Wave Open Science Center, to ensure that the data has the right quality, as well as spectrograms to discard clear noise anomalies. These lightweight post-processing analyses flagged 7 noise anomalies and 6 clean events. A sample is shown in figure 6, which presents spectrograms of a real event, GW200129_065458_1264314069, and a noise anomaly located at GPS time 1265332743.9816895.

4. Discussion

We have demonstrated how to encapsulate temporal and spatial aspects of gravitational wave detection into a novel spatiotemporal-graph AI model. We have tested this methodology considering a 4D signal manifold that describe binary black hole mergers. Our findings indicate that AI ensembles can attain optimal signal

Figure 6. Post-processing of noise triggers identified by AI ensemble. Spectrograms of a noise anomaly at GPS time 1265332743.9816895 (top panel), and the gravitational wave event GW200129_065458_1264314069 (bottom panel).

detection while also reducing the number of false positives to only 2 over a decade of searched data that describes a three detector network. This is the first time AI attains this level of accuracy and sensitivity for gravitational wave detection.

On the algorithm side of things, this work also represents a milestone in the training of AI models that combine hybrid dilated convolution networks and graph neural networks, since we succeeded in training these complex models at scale using up to 256 A100 GPUs with optimal performance, and demonstrated strong scaling using up to 512 A100 GPUs.

In addition to reducing time-to-solution using distributed training, we also distributed AI inference so as to process an entire decade of advanced gravitational wave data within 3.5 h. In brief, AI provides a natural pathway to accelerate and automate gravitational wave discovery using existing supercomputing resources.

We have explored the use of these AI ensembles to search for gravitational waves in O3b data available the Gravitational Wave Open Science Center. We did this by processing Advanced LIGO and Advanced Virg data that span the month of February 2020. Our findings indicate that we can indeed identify 6 HLV events that span the signal manifold used to train our AI ensembles, and readily discard noise anomalies. This is the first analysis in the literature that introduces AI models trained with higher order wave modes for an astrophysical population of quasi-circular, spinning, non-precessing binary black hole mergers.

Using real data, we identified a number of challenges related to the disparate sensitivities of the HLV detector network. A potential approach for a more resilient AI architecture may consist of aggregating predictions from the H and L channels (since they have comparable sensitivity) to figure out whether a given signal is concurrently observed by the Advanced LIGO detectors, and then look at the output from Advanced Virgo. This third output may provide additional confidence for a detection if any of the Advanced LIGO detectors is down and the signal is also visible in Advanced Virgo. However, AI predictions from advanced Virgo may not be used to discard potential events if they are not clearly extracted from Advanced Virgo data. This condition may be used to design AI models that consider a larger detector network, and may be relaxed once all detectors reach comparable sensitivity.

We also compared the performance of our AI ensemble with production scale analyses done with established gravitational wave pipelines, and then conducted a search for 10 gravitational wave sources using available gravitational wave data as is. These comparisons elucidated the strengths and weaknesses of each approach, and indicated that AI methods will greatly benefit from using information regarding data calibration, data quality input, and data cleaning. These additional pre-processing analyses should be incorporated in future AI analyses.

On the algorithm side of things, the choice of pooling operations in the GNN block can influence the quality of the learned node representations and ultimately affect the performance of our AI models. Currently, we are utilizing max pooling based on our preliminary ablation experiments with addition, max pooling, and average pooling. The specific nature of signal detection seems to favor max pooling since it provides best convergence and evaluation performance. However, in future work it will be worth exploring the idea of integrating multiple pooling strategies and concatenating their outputs. This approach may allow the model to capture a more comprehensive set of features and potentially generalize better.

This work sets the stage for the development of resilient AI approaches for signal detection using open source data at the Gravitational Wave Open Science Center to process Advanced LIGO and Advanced Virgo data at scale. The next frontier is the development of such AI models considering higher order wave modes that describe spinning and precessing binary black hole mergers.

Data availability statement

We produced datasets of modeled waveforms using IMRPhenomXPHM model [48], and recolored gravitational wave noise using the open source PyCBC library [50]. The Power Spectral Density noise curves for Advanced LIGO (aligo_O4high.txt), and Advanced Virgo (avirgo_O5low_NEW.txt) are readily available at the LIGO Document Control Center Portal [55]. The data that support the findings of this study are openly available at the following URL/DOI: https://github.com/mtian8/gw_spatiotemporal_gnn.

Acknowledgments

Contributions

E A H envisioned and led this work, and guided the design of AI models. M T designed novel approaches to develop the neural networks introduced in this article, and tested their performance with a variety of uncertainty quantification metrics. H Z distributed the training and inference of AI models in the Polaris supercomputer. P K carried out the PyCBC searches with open source data. All authors contributed to the writing and reviewing of this manuscript.

Code availability

The scientific software to reproduce our results, including data, AI models for synthetic and real noise, postprocessing code, and a tutorial for their use is available at GitHub [62].

ORCID iDs

Minyang Tian ⬡ https://orcid.org/0000-0001-8009-9116
E A Huerta ⬡ https://orcid.org/0000-0002-9682-3604
Huihuo Zheng ⬡ https://orcid.org/0000-0001-9008-9552

References

[1] Abbott B P *et al* 2017 *Astrophys. J. Lett.* **848** L12
[2] Evans M *et al* 2021 arXiv:2109.09882
[3] Bailes M *et al* 2021 *Nat. Rev. Phys.* **3** 344–66
[4] Maggiore M *et al* 2020 *J. Cosmol. Astropart. Phys.* JCAP03(2020)050
[5] Usman S A *et al* 2016 *Class. Quantum Grav.* **33** 215004
[6] Cannon K *et al* 2021 *SoftwareX* **14** 100680
[7] George D and Huerta E A 2018 *Phys. Rev.* D **97** 044039
[8] George D and Huerta E A 2017 Deep learning for real-time gravitational wave detection and parameter estimation with LIGO data *NiPS Summer School 2017* (arXiv:1711.07966)
[9] George D and Huerta E A 2018 *Phys. Lett.* B **778** 64–70
[10] Gabbard H, Williams M, Hayes F and Messenger C 2018 *Phys. Rev. Lett.* **120** 141103
[11] Lin Y C and Wu J H P 2021 *Phys. Rev.* D **103** 063034
[12] Wang H, Wu S, Cao Z, Liu X and Zhu J Y 2020 *Phys. Rev.* D **101** 104003
[13] Fan X, Li J, Li X, Zhong Y and Cao J 2019 *Sci. China Phys. Mech. Astron.* **62** 969512
[14] Li X R, Babu G, Yu W L and Fan X L 2020 *Front. Phys.* **15** 54501
[15] Deighan D S, Field S E, Capano C D and Khanna G 2021 *Neural Comput. Appl.* **33** 13859–83
[16] Rebei A, Huerta E A, Wang S, Habib S, Haas R, Johnson D and George D 2019 *Phys. Rev.* D **100** 044025
[17] Beheshtipour B and Papa M A 2020 *Phys. Rev.* D **101** 064009
[18] Schäfer M B and Nitz A H 2022 *Phys. Rev.* D **105** 043003
[19] Schäfer M B, Zelenka O, Nitz A H, Ohme F and Brügmann B 2022 *Phys. Rev.* D **105** 043002
[20] Gunny A, Rankin D, Krupa J, Saleem M, Nguyen T, Coughlin M, Harris P, Katsavounidis E, Timm S and Holzman B 2022 *Nat. Astron.* **6** 529–36

[21] Schäfer M B *et al* 2023 *Phys. Rev.* D **107** 023021
[22] Andrews M, Paulini M, Sellers L, Bobrick A, Martire G and Vestal H 2022 arXiv:2207.04749
[23] Yu H and Adhikari R X 2022 *Front. Artif. Intell.* **5** 811563
[24] Moreno E A, Borzyszkowski B, Pierini M, Vlimant J R and Spiropulu M 2022 *Mach. Learn. Sci. Tech.* **3** 025001
[25] Nemmen R, Duarte R and Navarro J P 2019 *Proc. Int. Astron. Union* **15** 329–33
[26] Övgün A, Sakallı I and Mutuk H 2021 *Int. J. Geom. Methods Mod. Phys.* **18** 2150154–2250
[27] Arraut I 2018 *Europhys. Lett.* **124** 50002
[28] Krastev P G 2020 *Phys. Lett.* B **803** 135330
[29] Schäfer M B, Ohme F and Nitz A H 2020 *Phys. Rev.* D **102** 063015
[30] Miller A L *et al* 2019 *Phys. Rev.* D **100** 062005
[31] Wei W and Huerta E A 2021 *Phys. Lett.* B **816** 136185
[32] Yu H, Adhikari R X, Magee R, Sachdev S and Chen Y 2021 *Phys. Rev.* D **104** 062004
[33] Qiu R, Krastev P G, Gill K and Berger E 2023 *Phys. Lett.* B **840** 137850
[34] Wei W, Huerta E A, Yun M, Loutrel N, Shaikh M A, Kumar P, Haas R and Kindratenko V 2021 *Astrophys. J.* **919** 82
[35] Huerta E A and Zhao Z 2021 Advances in machine and deep learning for modeling and real-time detection of multi-messenger sources *Handbook of Gravitational Wave Astronomy* (Springer) p 47
[36] Huerta E A *et al* 2019 *Nat. Rev. Phys.* **1** 600–8
[37] Burgazli A, Sergijenko O and Vavilova I 2022 Machine learning in cosmology and gravitational wave astronomy: recent trends *Horizons in Computer Science Research* vol 22 (Nova Science Publisher Inc.) pp 193–240
[38] Cuoco E *et al* 2021 *Mach. Learn.: Sci. Technol.* **2** 011002
[39] Huerta E A *et al* 2020 *J. Big Data* **7** 88
[40] Khan A, Huerta E A and Das A 2020 *Phys. Lett.* B **808** 135628
[41] Khan A, Huerta E A and Kumar P 2022 *Phys. Lett.* B **835** 137505
[42] Wei W, Khan A, Huerta E A, Huang X and Tian M 2021 *Phys. Lett.* B **812** 136029
[43] Huerta E A *et al* 2021 *Nat. Astron.* **5** 1062–8
[44] Chaturvedi P, Khan A, Tian M, Huerta E A and Zheng H 2022 *Front. Artif. Intell.* **5** 828672
[45] Razzano M and Cuoco E 2018 *Class. Quantum Grav.* **35** 095016
[46] Lee J, Oh S H, Kim K, Cho G, Oh J J, Son E J and Lee H M 2021 *Phys. Rev.* D **103** 123023
[47] Wei W and Huerta E A 2020 *Phys. Lett.* **B800** 135081
[48] Pratten G *et al* 2021 *Phys. Rev.* D **103** 104056
[49] Abbott R *et al* (KAGRA, VIRGO, LIGO Scientific) 2023 *Astrophys. J. Suppl.* **267** 29
[50] Nitz A H *et al* 2021 PyCBC. free and open software to study gravitational waves
[51] Vallisneri M, Kanner J, Williams R, Weinstein A and Stephens B 2015 *J. Phys.: Conf. Ser.* **610** 012021
[52] Abbott R *et al* (LIGO Scientific, VIRGO, KAGRA) 2021 arXiv:2111.03606
[53] Khan S, Husa S, Hannam M, Ohme F, Pürrer M, Jiménez F X and Bohé A 2016 *Phys. Rev.* **D93** 044007
[54] Abbott B P *et al* 2020 *Living Rev. Relativ.* **23** 3
[55] LIGO Document Control Center Portal 2022 Noise curves used for simulations in the update of the observing scenarios *Paper* (available at: https://dcc.ligo.org/LIGO-T2000012/public)
[56] van den Oord A, Dieleman S, Zen H, Simonyan K, Vinyals O, Graves A, Kalchbrenner N, Senior A and Kavukcuoglu K 2016 WaveNet: a generative model for raw audio *9th ISCA Speech Synthesis Workshop* p 125
[57] Bruna J, Zaremba W, Szlam A and Lecun Y 2014 Spectral networks and locally connected networks on graphs *Int. Conf. on Learning Representations (ICLR2014), CBLS*
[58] Gilmer J, Schoenholz S S, Riley P F, Vinyals O and Dahl G E 2017 Neural message passing for quantum chemistry *Int. Conference Machine Learning* (PMLR) pp 1263–72
[59] Hamilton W, Ying Z and Leskovec J 2017 Inductive representation learning on large graphs *Advances in Neural Information Processing Systems* vol 30, ed I Guyon, U V Luxburg, S Bengio, H Wallach, R Fergus, S Vishwanathan and R Garnett (Curran Associates, Inc.)
[60] Velickovic P *et al* 2017 *Stat* **1050** 10–48550
[61] Xu K, Hu W, Leskovec J and Jegelka S 2019 How powerful are graph neural networks? *Int. Conf. on Learning Representations*
[62] Minyang T and Huerta E A 2023 Physics-inspired spatiotemporal-graph AI ensemble for gravitational wave detection (available at: https://github.com/mtian8/gw_spatiotemporal_gnn)